Niklas, A., Santos, F., Gonzalez-Martinez, R. et al. Effects of Different Si Content and Thermal Stories on the Secondary Phase Formation, Hot Ductility, and Stress Rupture Properties of Alloy 718 Investment Castings. Metall Mater Trans A 54, 2670–2688 (2023). https://doi.org/10.1007/s11661-023-07046-4

ORIGINAL RESEARCH ARTICLE

Effects of Different Si Content and Thermal Stories on the Secondary Phase Formation, Hot Ductility, and Stress Rupture Properties of Alloy 718 Investment Castings

ANDREA NIKLAS, FERNANDO SANTOS, RODOLFO GONZALEZ-MARTINEZ, PEDRO PABLO RODRÍGUEZ, DANIEL BERNAL, ALBERTO COBOS, LEXURI VÁZQUEZ, and PEDRO ÁLVAREZ

Herein, the effects of microstructure on high-temperature properties (hot ductility and stress rupture life) were investigated in alloy 718 investment castings manufactured with different Si contents (0.051, 0.11, and 0.17 wt pct) and different cooling rates (0.52 °C/s and 1.65 °C/s). For the casting with a low cooling rate, an additional solution treatment step was added to the standard pre-weld heat treatment. Even small amounts of residual Laves phase (0.14 to 0.35 wt pct) adversely affected both the hot ductility and stress rupture properties. Hot ductility tests indicated that the presence of Laves phase led to an earlier decrease in hot ductility in on-heating tests and retarded ductility recovery in on-cooling tests. Both effects are usually associated with poorer weldability and greater hot cracking susceptibility. Ductility recovery was also affected by grain size and aspect ratio: columnar and smaller grain sizes showed better ductility recovery behavior. Stress rupture tests indicated that stress rupture life and elongation decreased with increasing Si content, due to the presence of a semicontinuous network of Laves phase at grain boundaries instead of intergranular δ phases. This effect was much more pronounced in stress rupture than in hot ductility tests. The presence of residual Laves phase was associated with higher Si content and lower cooling rates. The additional solution treatment step of 2 hours at 1052 °C did not eliminate the Laves phase completely.

https://doi.org/10.1007/s11661-023-07046-4

I. INTRODUCTION

ALLOY 718 is the most widely used Ni-based superalloy, because of its outstanding mechanical performance at working temperatures as high as 700 °C under high structural loading and corrosive conditions.[1] It was originally developed in the wrought condition by Eiselstein from the International Nickel Company in 1958. Currently, it is widely used in investment casting parts. Its remarkable mechanical strength at high temperatures is attributed to the precipitation of Nb-rich γ'' (Ni_3Nb) and γ' (Ni_3Al and $Ni_3(Ti, Al)$). These coherent precipitates strengthen the FCC γ matrix composed of Ni, Cr, and Fe.[1]

The plate or needle-shaped δ phase (Ni_3Nb) can form during solidification or solution heat treatment, or after prolonged exposure at high temperatures above the working temperature, due to transformation of the metastable γ'' phase, thus decreasing the mechanical properties of alloy 718. The δ phase is found primarily as plates growing on the (111) planes or nucleating at grain boundaries. The microstructure of alloy 718 can also be composed of carbides (Nb(Ta)C, TiC, M_6C), nitrides (TiN), and Laves and sigma phases. Carbides and nitrides are considered inert, but the topologically closely packed (TCP) phases, Laves, and sigma phases impair the mechanical properties.[1,2] Moreover, the formation of these phases during solidification decreases the content of Nb in the matrix and hinders the precipitation of desired γ'' precipitates. Finally, these

ANDREA NIKLAS, FERNANDO SANTOS, and RODOLFO GONZALEZ-MARTINEZ are with the Fundación AZTERLAN, Basque Research and Technology Alliance (BRTA), Aliendalde Auzunea 6, 48200 Durango, Spain. Contact e-mail: rgonzalez@azterlan.es PEDRO PABLO RODRíGUEZ is with the EIPC RESEARCH CENTER, AIE, Torrekua 3, 20600 Eibar, Spain. DANIEL BERNAL is with the Advanced Material Forming Processes, Mondragon University - Faculty of Engineering, Loramendi, 4, 20500 Arrasate - Mondragón, Spain. ALBERTO COBOS, LEXURI VÁZQUEZ, and PEDRO ÁLVAREZ are with the LORTEK Technological Centre, Basque Research and Technology Alliance (BRTA), 20240 Ordizia, Spain.
Manuscript submitted October 26, 2022; accepted March 28, 2023.
Article published online April 15, 2023

phases may induce incipient melting during high-temperature exposure and cause hot cracking during welding, because they have lower melting points than the matrix. The incipient melting temperatures associated with the presence of Laves phases have been reported to be between 1160 °C and 1180 °C[3–5] for alloy 718.

The Laves phase has Fe, Ni, Cr, Nb, and Ti atoms in its structure, and its stoichiometric chemical formula is $(Fe,Ni,Cr)_2(Nb,Ti)$. The formation of Laves and M_6C phases is usually associated with high Si content and high-temperature homogenization heat treatments. Thus, current manufacturing process specifications have been designed to avoid the formation of these detrimental phases by limiting Si content and homogenization temperatures.[6]

The precipitation of secondary phases, such as carbides, nitrides, and Laves phases, highly depends on the segregation of chemical elements, particularly Nb, Mo, and Ti, during solidification from the liquid state. Segregation of Nb is the main determinant of the presence of some of these phases in the final solidification microstructure. Segregation during the casting process directly depends on the cooling rate: faster cooling rates lead to a finer dendritic structure that affords better homogenization. The solidification of alloy 718 starts at approximately 1360 °C with the formation of lean austenitic dendrites depleted in Nb, Ti, and Mo, which migrate to the liquid located in interdendritic regions. Local enrichment in these elements leads to the formation of the described secondary phases between dendrites. Solidification is completed at approximately 1180 °C with the formation of γ/Laves eutectic from the terminal liquid. Further cooling in the solid-state promotes the precipitation of the δ phase (6 to 8 pct Nb) below 1050 °C, of the γ'' phase (4 pct Nb) at 960 °C to 700 °C and finally of the γ' phase at approximately 750 °C.[2]

The Laves phase generated after casting impairs the high-temperature mechanical properties of alloys 718; therefore, this phase must be dissolved during the manufacturing process through dedicated thermal treatments. In fact, to ensure the high structural performance at temperatures from 450 °C to 700 °C, the γ'' and γ' phases must be the prevalent and stable phases. Therefore, the Laves phase must be dissolved through adequate homogenization at temperatures from 1065 °C to 1080 °C for long soaking times before completion of the precipitation aging treatment.

The formation and presence of secondary phases also greatly influences the weldability properties of alloy 718. This property is very important, because many parts, such as gas turbine blades and hot parts of aircraft engines, must be joined or repaired during the manufacturing process. Good weldability properties arise from the slow γ'' (Ni_3Nb) precipitation kinetics compared to that of γ' (Ni_3Al and $Ni_3(Ti, Al)$) in precipitation-hardened alloys.

Susceptibility to liquation cracking during welding is commonly evaluated with the hot ductility (Gleeble) test.[7–11] In this test, both strength and ductility are measured at high temperatures. Data are obtained by testing samples after heating them to different temperatures (on-heating) and cooling them down from a given peak temperature (on-cooling). The temperature at which a metal alloy completely loses its strength, while it is heated under a constant tensile load, is called the nil strength temperature (NST). The nil ductility temperature (NDT) refers to the peak temperature at which the area reduction of the surface after breaking is 0 pct, whereas the ductility recovery temperature (DRT) is the temperature at which 5 pct of the area reduction is recovered after cooling from a temperature close to the NST. The DRT is determined from on-cooling testing conditions; in this case, strain is applied only when the final testing temperature has been reached.

Thompson *et al.*[7] have studied the effects of different heat treatments (as-received, solution annealed, and age hardened) on the hot ductility of wrought 718 alloy and have found that the solution heat treatment results in a microstructure that rapidly recovers ductility during on-cooling tests; therefore, this material is considered to have elevated resistance to hot cracking during welding. The role of heat treatment in the decreased on-cooling ductility recovery has been suggested to be associated with the amount and distribution of Nb on the liquated grain boundaries. Furthermore, eutectic Laves phases have been found adjacent to NbC precipitates, as an artifact of the cooling process[7,10] caused by constitutional liquation of NbC. Anderson *et al.*[10] have suggested that the numerous eutectic Laves islets are responsible for the decrease in the on-cooling ductility of alloy 718.

Andersson *et al.*[10,11] have studied the effects of different solution heat treatments on hot ductility in wrought alloy 718 and Allvac 718Plus with the hot ductility (Gleeble) test. They have concluded that constitutional liquation of NbC assisted by the δ phase occurs and deteriorates the ductility. The Laves phase was not observed in any heat treatment conditions in the parent material. Ductility loss was observed in the coarse grain size state, whereas the material with high amounts of δ phase on the grain boundary showed an increase in ductility because of a grain boundary pinning effect. Decreased on-cooling ductility was attributed to the accumulation of trace elements on grain boundaries.

The influence of homogenization treatments on hot ductility in cast 718 and cast ATI® 718Plus®, as well as the effects of Nb and minor elements on liquation characteristics, have been studied by Singh *et al.*[9,12] For both alloys, the extent of liquation was found to determine the hot ductility of the material. Enhanced homogenization of Nb decreased the solidus temperature, thus leading to extensive melting of grain boundaries in the long dwell time heat treatments (1190 °C/24 hours). This aspect might have been further facilitated by the presence of minor elements such as Si, S, P, and B contributing to the suppression of the liquation temperature along the grain boundaries. For the heat treatment at lower temperature and shorter time (1120 °C/4 hours), liquation was caused primarily by melting of the partially dissolved Laves phase and constitutional liquation of MC carbides. The heat treatment at 1190 °C/4 hours, without Laves phases,

exhibited extensive constitutional liquation of NbC carbides and partial grain boundary melting.

Apart from the requirement for good weldability, the application of alloy 718 castings in the aircraft engines requires elevated creep and stress rupture properties. The effects of the minor elements P, S, and Si on the microstructure and stress rupture properties in wrought 718 alloy have been investigated by Guo *et al.*[13] In that study, S and Si had no notable effects on the stress rupture properties in the tested range, whereas a peak in stress rupture life and ductility was achieved at 0.013 wt pct P. When the Si content was raised from 0.024 to 0.035 pct, the formation of Laves and MC phases on the grain boundaries increased while the precipitation of δ phase decreased. Despite the presence of harmful Laves phases at the grain boundaries, no decrease in stress rupture properties was observed, due to increased oxidation resistance. In addition, Schirra *et al.*[14] have investigated the effects of Si content on Laves phase formation and stress rupture properties in wrought 718. They have observed that the amount of intergranular Laves phase increases as the Si content is raised from 0.11 to 0.30 wt pct. However, rupture and creep life were not affected by the presence of these residual amounts of Laves phase at grain boundaries but appeared to be strongly associated with the grain size.

The negative effect of the Laves phases on the mechanical properties at room temperature (ultimate tensile strength and ductility), the stress rupture properties (rupture life and elongation) and the elevated temperature fatigue crack growth resistance in cast + HIP alloy 718 has been investigated by Schirra *et al.*[14] In that study, cast bars were slowly solidified (2 °C/minutes) over a range from 1371 °C to 1177 °C to attain high levels of Laves phase in the microstructure, thus resulting in the precipitation of large globular aggregates in the interdendritic regions. Examination of stress rupture properties indicated that the material with high Laves content exhibited a 2.4 times lower in rupture life and a 1.6 times lower rupture elongation than the Laves-free material.

Finally, the influence of Laves phases on the room temperature tensile, creep, and thermomechanical fatigue of Inconel 718 fabricated through different additive manufacturing processes, *i.e.*, powder bed fusion and directed energy deposition, has recently been studied in detail.[15–17] Despite the extremely high cooling rates and rapid solidification during additive manufacturing processes, which results in fewer segregation issues than investment casting, the microstructure of as-built additive manufactured components usually contains Laves phases that must be dissolved by dedicated thermal treatments to ensure good tensile strength, ductility, fatigue, and creep properties. In terms of ductility, granular Laves phases have been found to be more favorable than long striped Laves phases. Moreover, improvements in creep properties after heat treatment have been associated with the dissolution of Laves phase and precipitation of δ-phase plates, which avoid motion of dislocations.

The aim of the present work was to advance knowledge and understanding of the effects of small amounts of residual Laves phases on the high-temperature properties of alloy 718 investment castings. Minor amounts of Laves phases with different morphologies and distributions (interdendritic region and grain boundaries) were obtained by varying the Si content and solidification rate and adding another solution heat treatment to the conventional pre-weld heat treatment. In terms of hot ductility, this work completes the analysis of the weldability results published previously,[18] by analyzing the microstructures of tested samples. In the previous study, a hot cracking mechanism activated during laser beam welding of alloy 718 investment castings was described. This mechanism is more closely associated with the welding morphology than with the Si content and residual Laves phase resulting from different chemistries and thermal treatments.

II. EXPERIMENTAL

A. *Material*

Investment casting castings were manufactured by incorporation of 20 test samples as flat plates of 150 × 50 × 10 mm in each mold. The casting process was as previously described in detail.[18]

The chemical composition of the different castings is shown in Table I. Of note, casting O (low Si content) was manufactured by using high purity ingots as raw material. In casting P (high Si content), Si was intentionally added during vacuum melting, and chemically adjusted ingots (28 kg in total) were manufactured in a first melting step. Casting E corresponded to the conventional chemical composition and casting process, whereas the cooling rate during solidification was decreased in castings N and NP, with equivalent chemical composition, by incorporation of a ceramic blanket over the cast parts. The cooling rates between 800 °C and 500 °C, as experimentally determined by thermocouples, were 0.52 °C/second and 1.65 °C/

Table I. Chemical Compositions of Alloy 718 Casting Heats in Weight Percentages

Casting	Ni	C	Si	Mn	P	S	Fe	Cr	Mo	Ti	Al	Nb + Ta
O	51.9	0.047	0.051	< 0.050	< 0.010	< 0.005	21.1	17.8	3.02	0.89	0.47	4.75
E	52.1	0.049	0.11	0.037	< 0.010	< 0.005	20.4	17.6	2.91	0.98	0.59	4.92
P	51.7	0.038	0.17	< 0.050	< 0.010	< 0.005	21.1	17.7	3.02	0.89	0.46	4.85
N/NP	52.5	0.058	0.12	0.038	< 0.010	< 0.005	20.3	17.7	2.88	0.77	0.47	4.88

Table II. Heat Treatments for Cast Alloy 718, According to the *AMS 5383F:2018 Standard, and HIP Heat Treatment According to **Specification V.AC:9922 from GKN Aerospace Trollhättan (Sweden) and from ***Schirra[19]

Homogenization*	Pre-HIP	HIP**	Post-HIP**	Solution Heat Treatment*	Precipitation Heat Treatment***
1093 ± 14 °C/1 to 2 hours followed by air cooling	1052 ± 14 °C/2 hours followed by air cooling	1120 °C to 1170 °C 4 hours	1030 °C to 1080 °C 1 hour	954 ± 14 °C/1 hour followed by air cooling	760 ± 14 °C/5 hours cooled to 649 ± 14 °C/1 hour followed by air cooling

second for the molds with blanket (casting N/NP) and without blanket (casting O/E/P), respectively.

After the parts were shot blasted, they were subjected to the following heat treatment sequence: homogenization, pre-HIP, HIP, post-HIP, solution heat treatment, and short precipitation treatment (Table II). The homogenization and solution heat treatments were performed according to the AMS 5383F:2018 standard, whereas the HIP heat treatment was performed according to specification V.AC:9922 from GKN Aerospace Trollhättan (Sweden). Of note, to preserve confidentiality regarding the HIP treatment, only a temperature range can be given. An additional pre-HIP treatment consisting of solutionizing at 1052 °C for 2 hours followed by air cooling was applied only to the slowly cooled casting NP. The goal of this treatment was to dissolve residual Laves phases that remained present after the homogenization treatment. Unpublished results obtained in previous work performed with the rapidly solidified casting have indicated that this temperature is effective for dissolving residual Laves and also δ phases if present. The short two-step precipitation heat treatment, as reported by Schirra,[19] was performed only for the stress rupture tests to obtain the high mechanical properties at elevated temperatures, whereas the ductility tests were performed in the solution heat-treated state.

The different thermal conditions of the castings are summarized in Table III.

B. *Hot Ductility Tests*

Hot ductility tests of five casting heats were performed in a Gleeble 3800D thermomechanical simulator (DYNAMIC SYSTEMS INC., Poestenkill, NY, USA) owned by West University in Sweden. Here, 6 mm (− 0.025 mm, + 0.01 mm) diameter cylindrical shape samples were finely turned from 10 mm thickness casting plates after the corresponding thermal treatments. The test samples were extracted from the plate in the longitudinal direction. The hot ductility testing setup and guidelines included in the Gleeble Users Training 2010 handbook were applied. The sample geometry (Figure 1(a)) was comparable to that in the testing specifications included in procedure B of Reference [20] and differences in sample length were minimal. The NST temperature was determined only in casting E, focusing the overall hot ductility assessment of the five castings on on-heating and on-cooling tests. A heating rate of 111 °C/second from room to testing temperatures was used in on-heating tests, whereas samples were heated to 1195 °C at the same heating rate and subsequently cooled at 50 °C/second to the different testing temperatures used in the on-cooling trials (Figure 1(b)). Temperature profiles were recorded with a K-type thermocouple welded to the surface of each testing sample in the area between clamps. The samples were pulled to fracture at a 55 mm/second stroke rate. The percentages of area reduction from the initial 28.3 mm^2 (*i.e.*, 6 mm diameter) was measured to determine ductility at the different testing temperatures.

Table III. Thermal Conditions of the Castings

Casting	Cooling Rate	Solutionizing at 1052 °C/2 hours	HIP and Solution Heat Treatment
O, E, P	1.65 °C/second (without blanket)	no	yes
N	0.52 °C/second (with blanket)	no	yes
NP	0.52 °C/second (with blanket)	yes	yes

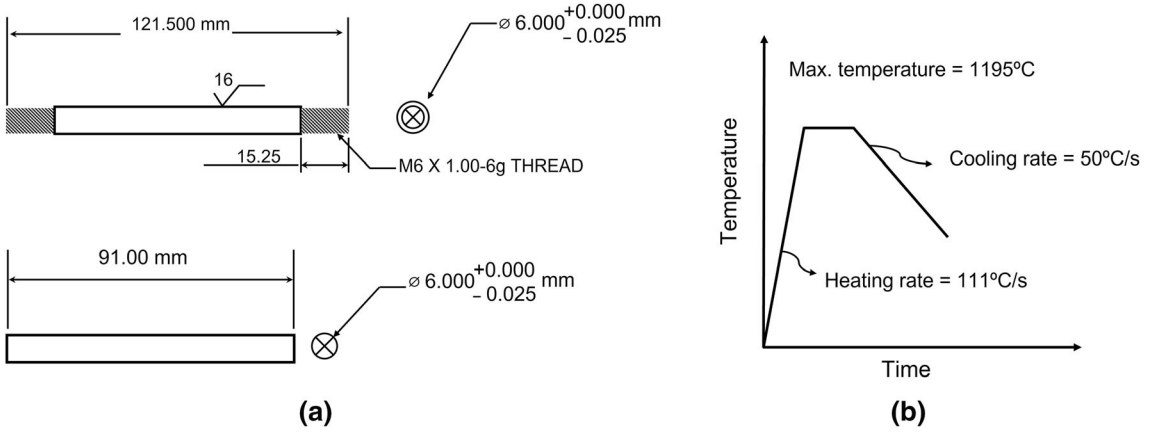

Fig. 1—(*a*) Hot ductility test sample geometry for on-heating and on-cooling tests (top), and NST tests (bottom) and (*b*) thermal cycle for on-cooling tests.

C. *Stress Rupture Tests*

Stress rupture tests were performed at a temperature of 650 °C with a constant stress of 689 MPa, according to standard ISO 204. A creep testing machine (T800), designed by SVÚM, a.s., Czech Republic, was used for the tests. The dimensions of the stress rupture test specimen are shown in Figure 2. The test samples were extracted from the plates in the longitudinal direction. This test was performed on the low silicon alloy (casting O) and high silicon alloy (casting P). Three specimens were tested for each alloy. Student's *t*-test was used to evaluate the differences in numerical results.

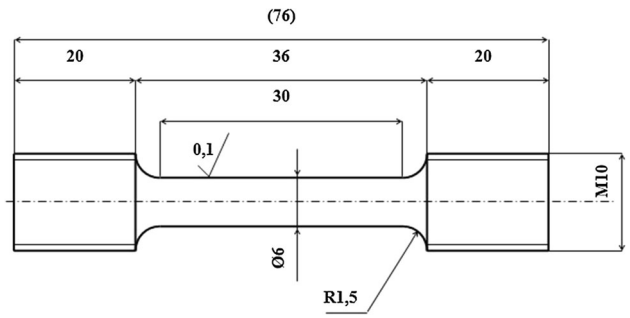

Fig. 2—Dimensions of the stress rupture test specimen.

D. *Microstructure Characterization*

Fracture surfaces and longitudinal sections of hot ductility and stress rupture test samples were characterized by field emission scanning electron microscopy (FESEM) with a ZEISS Ultra Plus microscope (CARL ZEISS AG, Oberkochen, Germany). Energy-dispersive X-ray (EDX) spectroscopy analysis was conducted with a field emission scanning electron microscope to determine the chemical compositions of precipitates and phases. The chemical composition of the Laves phases and other precipitates was determined through EDX analysis. For the metallographic analysis, longitudinal cross sections were prepared from the test samples by grinding and polishing through standard procedures. The area percentages of carbides were determined through the analysis of five images obtained by optical microscopy with a LEICA MEF4 microscope (LEICA MICROSYSTEMS GmbH, Wetzlar, Germany) at 100 times (HAZ and BM) in Leica application suite V4.2. The area percentages of Laves phases + carbides were determined through SEM at 500 times. Finally, the Laves phase area percentage was obtained by subtraction of the carbide area percentage obtained by optical microscopy from the area percentage of Laves phases + carbides obtained by SEM.

The grain size was revealed through etching of hot ductility on-cooling test samples by using Kalling 2 reagent. Dimensions of at least five grains were analyzed for each casting heat in the stereomicroscopy images obtained at 20 times. The grain size was determined from the horizontal and vertical mean intersection lengths between two grain boundaries.

The solidus and liquidus temperatures of the five castings were determined by thermodynamic calculation with Thermo-Calc software (using the TCNI10 and MOBNI4 databases) and experimentally through differential scanning colorimetry (DSC). Scheil simulations were performed at cooling rates of 1.65 °C/second and 0.52 °C/second, considering back diffusion of solute elements (Ni, C, Si, Mn, Fe, Cr, Mo, Ni, Ti, and Al) in

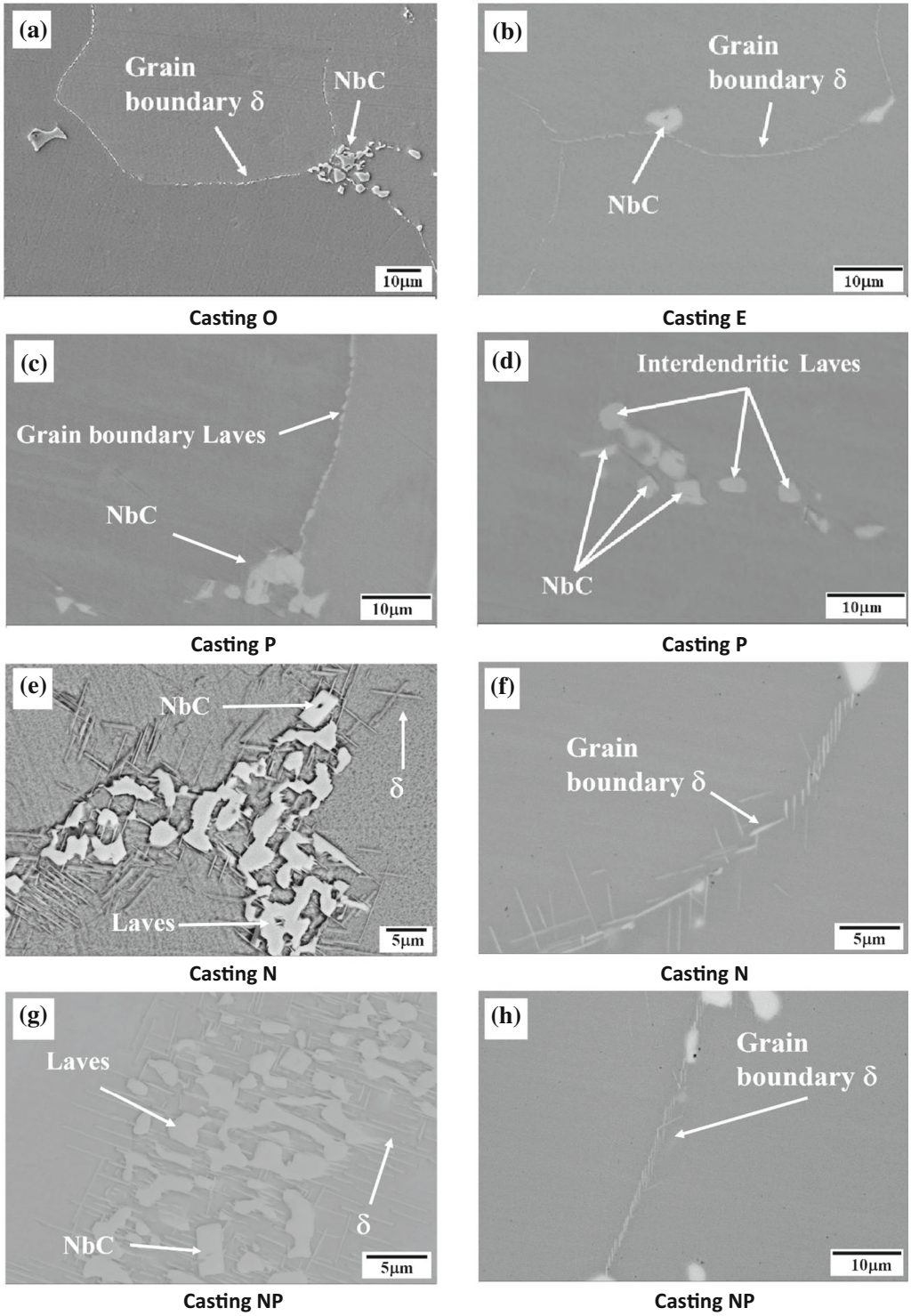

Fig. 3—Secondary phases observed in the base metal of (*a*) casting O, (*b*) casting E, (*c*) and (*d*) casting P, (*e*) and (*f*) casting N, (*g*) and (*h*) casting NP.

the primary phase. Additionally, C, as an interstitial element, was considered as fast diffuser. DSC measurements were performed with NETZSCH STA 449 F3 Jupiter DSC (NETZSCH, Selb, Germany) thermal analysis equipment at a constant heating/cooling rate of 10 °C/minute.

III. RESULTS

A. *Microstructures of the Base Metal*

The microstructures of the homogenization, HIP, and solution heat-treated base metal of the five castings are shown in Figure 3 and summarized in Table IV. The

main secondary phases observed in all samples are NbC carbides located on grain boundaries and in the interdendritic regions and δ phases along the grain boundaries, as well as minor amounts of TiMoC and carbosulfides.

Additionally, in casting P, which had the highest Si content, small residual amounts of Laves phases with globular morphology were also observed in the interdendritic regions (Figure 3(d)), as well as a semicontinuous network of fine elongated Laves phase along grain boundaries (Figure 3(c)). Likewise,[13,14] previous studies have indicated that in wrought 718 alloys with higher Si content, the grain boundary δ phase is substituted by a Laves phase. In the current study, both Laves and δ phases observed at the grain boundaries were likely to have precipitated during the solution treatment at 954 °C rather than during solidification process. The homogenization treatment + HIP treatments were performed at temperatures sufficiently high to rapidly dissolve such fine δ and Laves phases. The time–temperature–transformation (TTT) diagram of alloy 718[21] shows that precipitation of both phases occurs below 1050 °C. However, during the solution heat treatment at 954 °C for 1 hour, the δ phase shows a faster precipitation kinetics and thus no Laves phases would be expected in the microstructure.

Casting N and NP with low solidification rates revealed areas with accumulation of globular Laves phases, needle-shaped δ phases, and NbC carbides in the interdendritic regions formed due to segregation and a slow solidification rate (Figures 3(e) and (g)). Occasionally, these regions coincided with a grain boundary. In these strongly segregated regions, the applied homogenization, HIP, and solution heat treatments were apparently unable to dissolve the Laves and δ phases formed during the investment casting solidification process.

The area percentage of Laves before and after heat treatment is presented in Table V. Of note, casting P, which had the highest Si content, showed the highest Laves phase amount in the as-cast condition. Moreover, the heat treatment (homogenization, multi-stage HIP + solution heat treatment) dissolved the Laves phase in casting O and E, whereas in castings P, N, and NP, residual amounts of Laves phase remained present.

The grain sizes of the five castings are shown in Table VI. The grains of the slowly solidified casting N and NP were coarser and showed more equiaxed morphology, whereas grains in castings O, E, and P with standard cooling rates during solidification showed a marked columnar shape. Of note, the grain length and aspect ratio of the hot ductility test samples (transverse sections) were slightly smaller than those measured previously[18] on the original 10 mm thick plates (longitudinal sections), probably because the hot ductility test samples were machined to a diameter of 6 mm, and thus, part of the grains were cut off. Otherwise, no significant differences were observed between the transverse and longitudinal sections.

A more detailed description of microstructures (grain size, Laves phase composition, and microsegregation) of the five castings has been reported previously.[18]

Table IV. Secondary Phases and Their Locations, Observed in the Different Samples After Heat Treatment

Casting	NbC ID + GB	Globular Laves ID + GB	Fine Elongated Laves GB	δ ID	δ GB	Carbosulfide ID + GB	TiMoC ID + GB
O	x	—	—	—	x	x	x
E	x	—	—	—	x	x	x
P	x	x	x	—	x	x	x
N	x	x	—	x	x	x	x
NP	x	x	—	x	x	x	x

ID: interdendritic, GB: grain boundaryReprinted from Ref. [18], under the terms of the Creative Commons CC BY license.

Table V. Area Percentages of Globular Laves Phase in As-Cast Condition and After Heat Treatment [Homogenization (H), Hot Isostatic Pressing (HIP), Solution Heat Treatment (S)]

Casting	State	Area Percent Laves
O	as-cast	2.20
	H + HIP + post-HIP + S	*
E	as-cast	2.40
	H + HIP + post-HIP + S	*
P	as-cast	3.50
	H + HIP + post-HIP + S	0.35
N	as-cast	2.60
	H + HIP + post-HIP + S	0.19
NP	pre-HIP	2.10
	H + pre-HIP + HIP + post-HIP + S	0.14

Grain boundary Laves could not be quantified, because of their small size. Reprinted from Ref. [18], under the terms of the Creative Commons CC BY license.*Laves phase was not detected.

Table VI. Grain Size (Mean Width and Length with Standard Deviation) of Transverse (Hot Ductility Samples) and Longitudinal Sections (As-Cast Plate; Data Reprinted with Permission from Ref. [18], Under the Terms of the Creative Commons CC BY License)

Casting	Section	Mean Width (mm)	Mean Length (mm)	Aspect Ratio	Morphology
O	transverse	1.0 ± 0.16	3.0 ± 0.40	3.0	columnar
	longitudinal	1.1 ± 0.35	3.0 ± 0.92	3.1	columnar
E	transverse	0.7 ± 0.12	2.3 ± 0.18	2.9	columnar
	longitudinal	1.0 ± 0.46	3.2 ± 0.97	3.2	columnar
P	transverse	0.9 ± 0.25	2.6 ± 0.89	2.9	columnar
	longitudinal	1.1 ± 0.33	3.3 ± 0.78	3.0	columnar
N/NP	transverse	1.7 ± 0.26	2.5 ± 0.42	1.5	coarse, slightly columnar
	longitudinal	2.1 ± 0.34	3.4 ± 0.71	1.5	coarse, slightly columnar

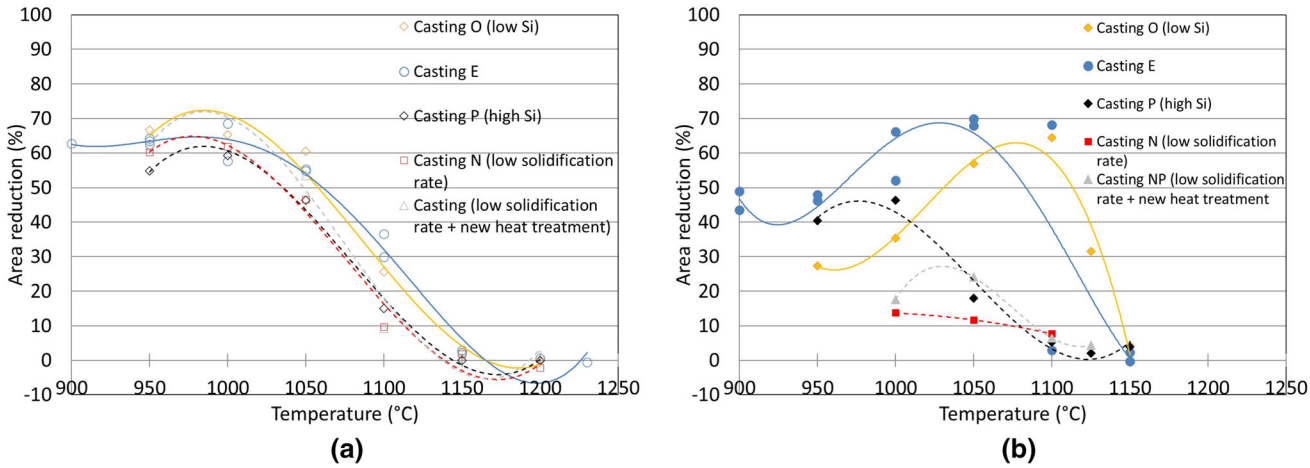

Fig. 4—Comparison of (*a*) on-heating and (*b*) on-cooling curves of castings E, O, P, N, and NP. (a) Reprinted from Ref. [18], under the terms of the Creative Commons CC BY license and (b) uses data from the same source.

B. *Hot Ductility*

Hot ductility curves of the five casting heats, determined in on-heating and on-cooling test conditions, are displayed in Figure 4. Samples were tested after HIP and solution heat treatment. The hot ductility curves depict the area reduction percentage measured in the broken samples tested at different temperatures. For the sake of comparison, grade 3 polynomial fitting of the experimental data was applied. The five castings showed high ductility (> 55 pct area reduction) at temperatures as high as 1000 °C. Castings E and O (low Si content) had comparatively higher values. Above 1000 °C, the ductility of every casting heat decreased rapidly to values near 0 pct at 1150 °C. At intermediate temperatures between 1000 °C and 1150 °C, castings E and O (low Si content) showed slightly better performance in terms of ductility; therefore, the fitting curves were somewhat displaced to the right, *i.e.*, to higher temperatures. Consequently, these two alloys had higher incipient melting temperatures.

The on-cooling curves showed more difference between castings than the on-heating curves. Casting O (low Si content) recovered ductility very quickly, reaching a 64 pct area reduction at 1100 °C. Notably, the thermal cycle in these on-cooling testing conditions entailed rapid heating to the peak soaking temperature of 1195 °C and subsequent rapid cooling to the testing temperatures. The peak temperature was selected based on NST values previously determined in casting E samples.[18]

As shown in Figure 4(b), the ductility recovery rate depended strongly on the Si content. The alloy with the lowest Si content (casting O) displayed a better and quicker ductility recovery behavior during on-cooling tests. The ductility recovery performance of castings N and NP, which had slower cooling rates during casting, was much poorer, and showed a very limited increase in area reduction at testing temperatures down to 1000 °C (Figure 4(b)). DRT and brittle temperature range (BTR) values, estimated from the hot ductility curves of the five castings, are shown in Table VII. BTR is a parameter usually used to analyze the hot cracking susceptibility of superalloys during welding.[9,20,22] It is defined as the difference between the peak temperature used in on-cooling tests and DRT, that is, the temperature at which a 5 pct area reduction is recovered again.

Table VII. Weldability Parameters Obtained from Hot Ductility tests

Casting	Peak Temperature (°C)	DRT (°C)	BTR (°C)	Maximum Ductility After Cooling	Ductility Recovery Rate
O	1195	1150	45	64 pct at 1100 °C	very fast
E	1195	1145	50	69 pct at 1050 °C	fast
P	1195	1090	105	46 pct at 1000 °C	intermediate
N	1195	1110	85	14 pct at 1000 °C	very low
NP	1195	1110	85	24 pct at 1050 °C	very low

Table VIII. Stress Rupture Properties of the Samples from Casting O (Low Si Content) and P (High Si Content)

Casting	Time to Rupture (hours)	σ (hours)	Elongation (Percent)	σ (Percent)	Reduction of Area (Percent)	σ (Percent)
O	65.25		3.37		6.90	
	57.25		3.37		10.11	
	46.00		4.60		10.18	
Average	56.17	9.67	3.78	0.71	9.06	1.87
P	43.50		4.04		4.73	
	28.25		2.00		5.20	
	41.75		3.20		5.99	
Average	37.83	8.35	2.60	0.85	5.30	0.64

Time to rupture and elongation are not statistically different.

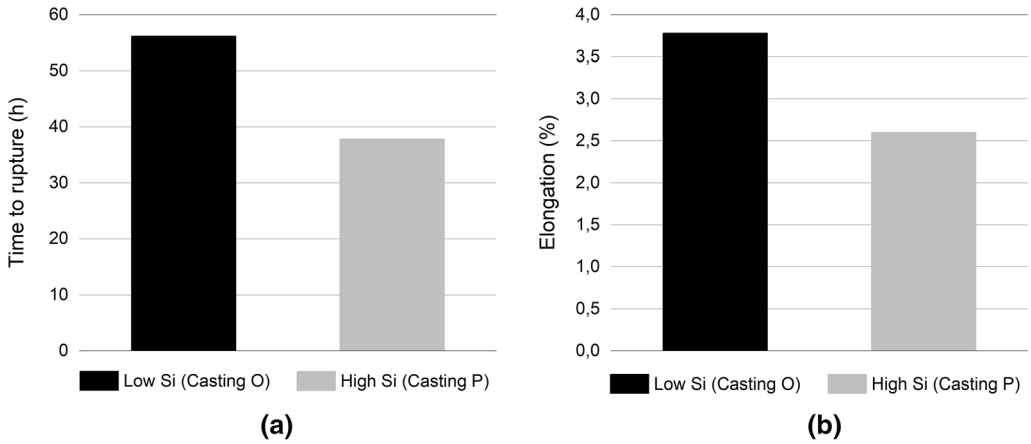

Fig. 5—Stress rupture properties: (*a*) time to rupture and (*b*) elongation of fully heat-treated (homogenization + HIP + post-HIP + solution heat treatment + precipitation heat treatment) Inconel 718 with low and high Si content.

C. *Stress Rupture Tests*

The stress rupture properties were determined on casting O (low Si) and P (high Si) and are presented in Table VIII and Figure 5. When the Si content increased from 0.051 to 0.17 wt pct, the rupture life, elongation, and percentage of area reduction decreased by 32.7 pct, 31.2 pct, and 41.5 pct, respectively.

IV. DISCUSSION

A. *Hot Ductility*

1. *On-heating tests*

Experimentally determined on-heating hot ductility curves are compared in Figure 4(a). Each sample from the five castings tested up to 1000 °C showed high ductility and area reduction percentages of 55 to 68 pct. In samples from castings N and NP, which had slower cooling rates during solidification, coarser and less columnar grains had lower area reduction values. The corresponding fracture surfaces of these samples (Figure 6) revealed a ductile failure mode dominated by microvoid coalescence. Fracture surfaces are comparable for the samples taken from different castings.

At 1100 °C, the area reduction decreased in all references to values between 26 and 37 pct in castings O (low Si) and E(medium Si), respectively, and between 9 and 15 pct in castings P (high Si), N, and NP (slow solidification rate), which had residual Laves phase in their microstructures after heat treatment. The

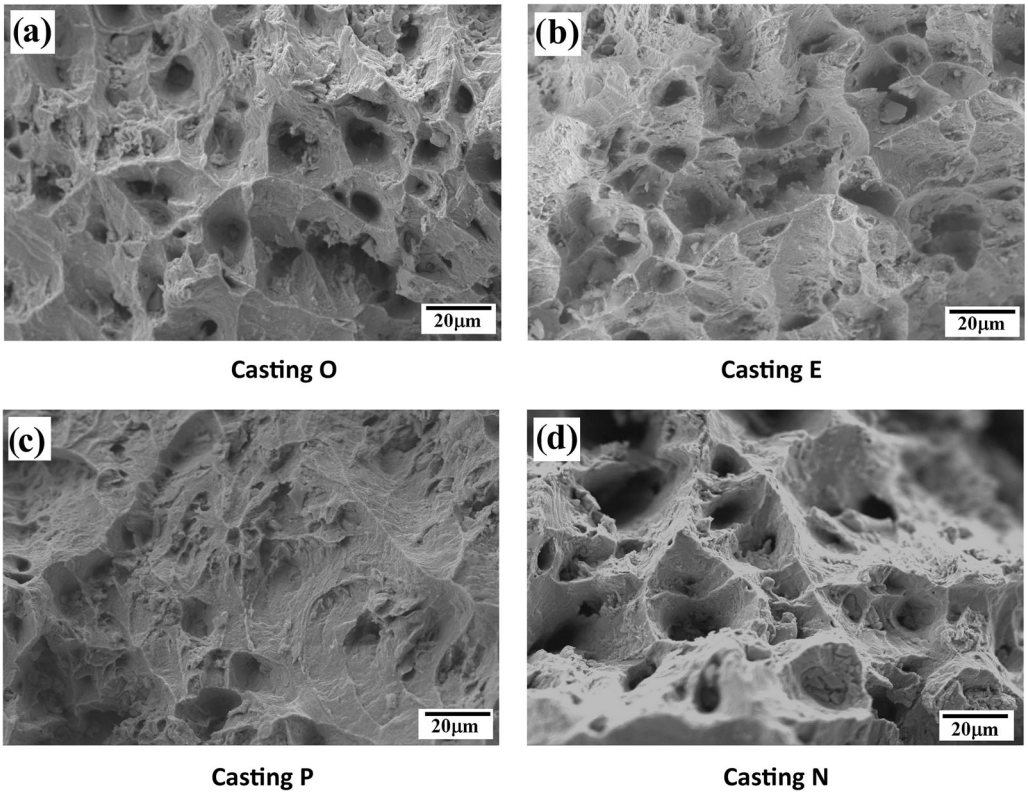

Fig. 6—Fracture surfaces of on-heating samples pulled at 1000 °C: (*a*) casting O, (*b*) casting E, (*c*) casting P, and (*d*) casting N.

corresponding fracture surfaces of these samples (Figure 7) showed a smoother morphology and less evidence of microvoids than fracture surfaces of castings tested at 1000 °C, particularly in castings P, N, and NP (Figures 7(c) through (e)).

At 1150 °C, hot ductility was completely lost in the five castings heats. The fracture surfaces at this testing temperature (Figure 8) revealed a smooth morphology indicating extensive grain boundary melting and the presence of unreacted carbides in every sample.

As summarized in Table V, the amount of Laves phase measured in castings N, NP, and P in the solution-annealed condition was between 0.14 and 0.35 pct. In the samples from these three castings, the onset of the ductility decrease during on-heating hot ductility tests was triggered at slightly lower temperatures, and corresponding fitting curves were marginally displaced to the left (Figure 4(a)). Notably, the dashed lines in Figure 4 indicate the trends of these three castings with residual Laves phase content. This early loss of ductility is associated with incipient melting of Laves phase, which is a rapid event that does not require a substantial reaction time to form the liquid, in contrast to constitutional liquation of NbC.[22,23] Therefore, the Laves phase can readily melt upon heating at very fast rates, such as those used in the current hot ductility tests (111 °C/second). The Laves phase impairs both weldability and the mechanical properties of alloy 718, as often reported in castings with substantial volume fractions of Laves phase and NbC.[6,24]

2. *On-cooling tests*

Differences in hot ductility performance among the five castings were much more evident in on-cooling than on-heating curves (Figure 4(b)) and corresponding microstructures. At the highest testing temperatures, grain boundary melting was observed in the microstructure, thereby resulting in a brittle fracture without any measurable area reduction. Castings O (low Si) and E (medium Si), both of which were free of Laves phase in the parent base metal, had relatively shorter BTR and faster ductility recovery rates. In these two castings, ductility was fully recovered at temperatures close to 1100 °C, reaching the original values well above 60 pct of the area reduction (Table VI). Fracture surfaces of samples tested at 1100 °C (casting O) and 1050 °C (casting E) revealed ductile fracture by void coalescence (Figure 9).

In contrast, castings N and NP were characterized by high BTR (85 °C), and very low ductility recovery rate and capability, with very low area reduction percentages (< 25 pct) even at low temperatures. The fracture surfaces of these castings showed the persistence of a liquid film at grain boundaries, even at 1000 °C (Figures 10(d) and (e)). Thompson *et al.*[7] have reported that the ductility loss during cooling in alloy 718 increases proportionally to the volume of intergranular liquid formed during heating. This extremely limited ductility recovery behavior is suggested to be due to the coarser grain sizes observed in these two heats with slower solidification cooling rates, as previously

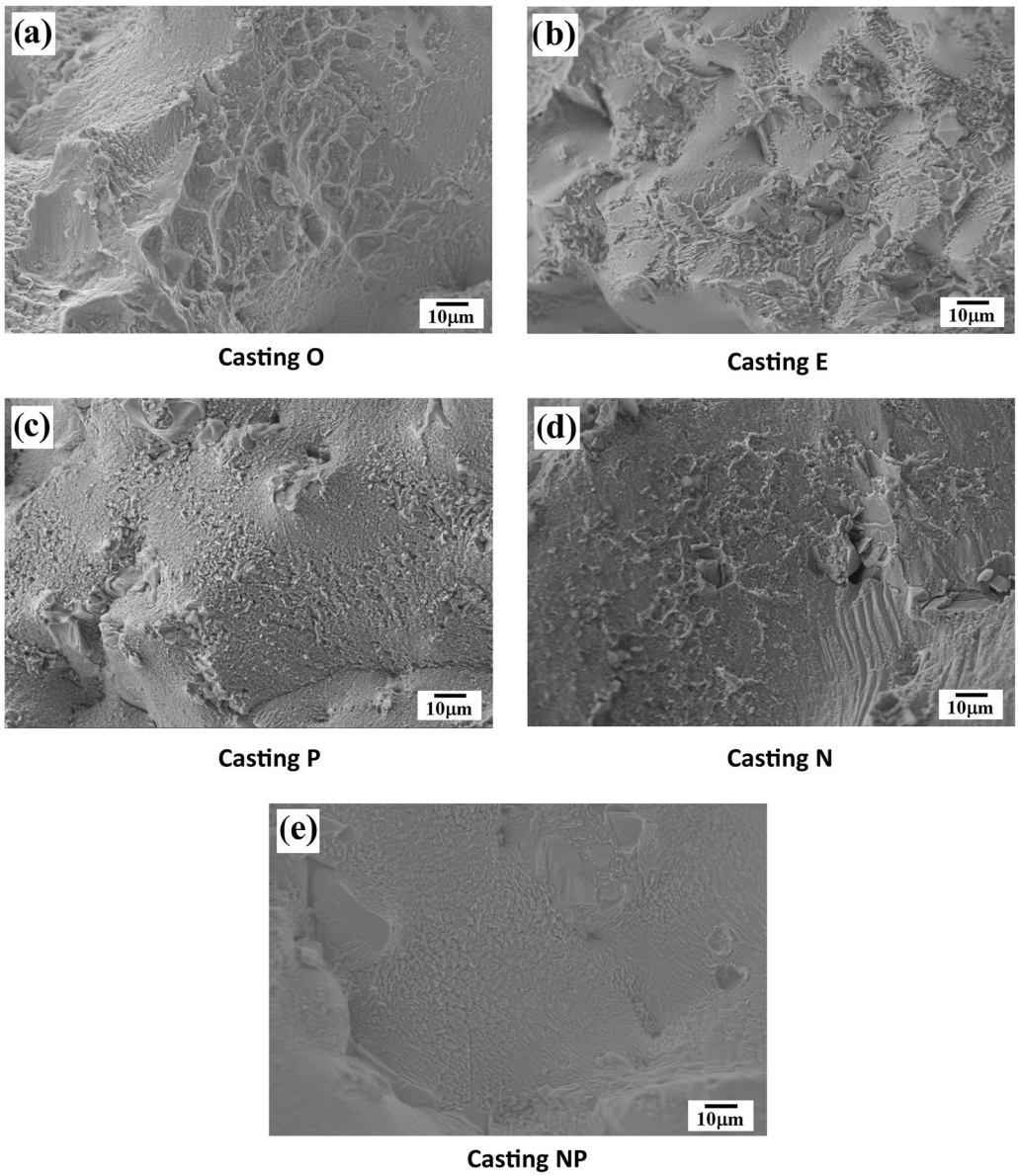

Fig. 7—Fracture surfaces of on-heating samples pulled at 1100 °C: (*a*) casting O, (*b*) casting E, (*c*) casting P, (*d*) casting N, and (*e*) casting NP.

described in detail.[18] Large grain sizes enhance the continuity of liquid resulting from incipient melting at grain boundaries, thereby decreasing the interfacial area between solid-state γ grains.[22]

Finally, casting P (high Si content) had the widest BTR (105 °C) and showed intermediate recovery rate and capability with respect to the other castings. Extended BTR was associated with higher amounts of residual Laves phase observed as a semicontinuous network along grain boundaries before testing (Tables IV and V). The effect of Si content on HAZ cracking of 718 alloys was previously investigated, it has been concluded that HAZ cracking is favored if high Si content is combined with high Mn or C content, due to the decrease in solidus temperature.[2,6] Therefore, both the semicontinuous film of Laves phase on grain boundaries and the higher Si content contributed to increasing the volume fraction of intergranular liquid formed at the peak temperature of 1195 °C in casting P samples. The fracture surfaces of the sample from the casting pulled at 1050 °C showed areas with ductile fracture mode and isolated smooth areas indicating the presence of liquid film (Figures 9(c) through (e)). In the smooth areas also, indications for constitutional NbC liquation were observed, showing Nb-enriched areas close to NbC carbides (Figures 9(d) and (e)).

At 1000 °C, ductility was largely recovered in castings O, E, and P, whereas the slowly solidified castings N and NP showed still the presence of liquid film on the fracture surface (Figure 10).

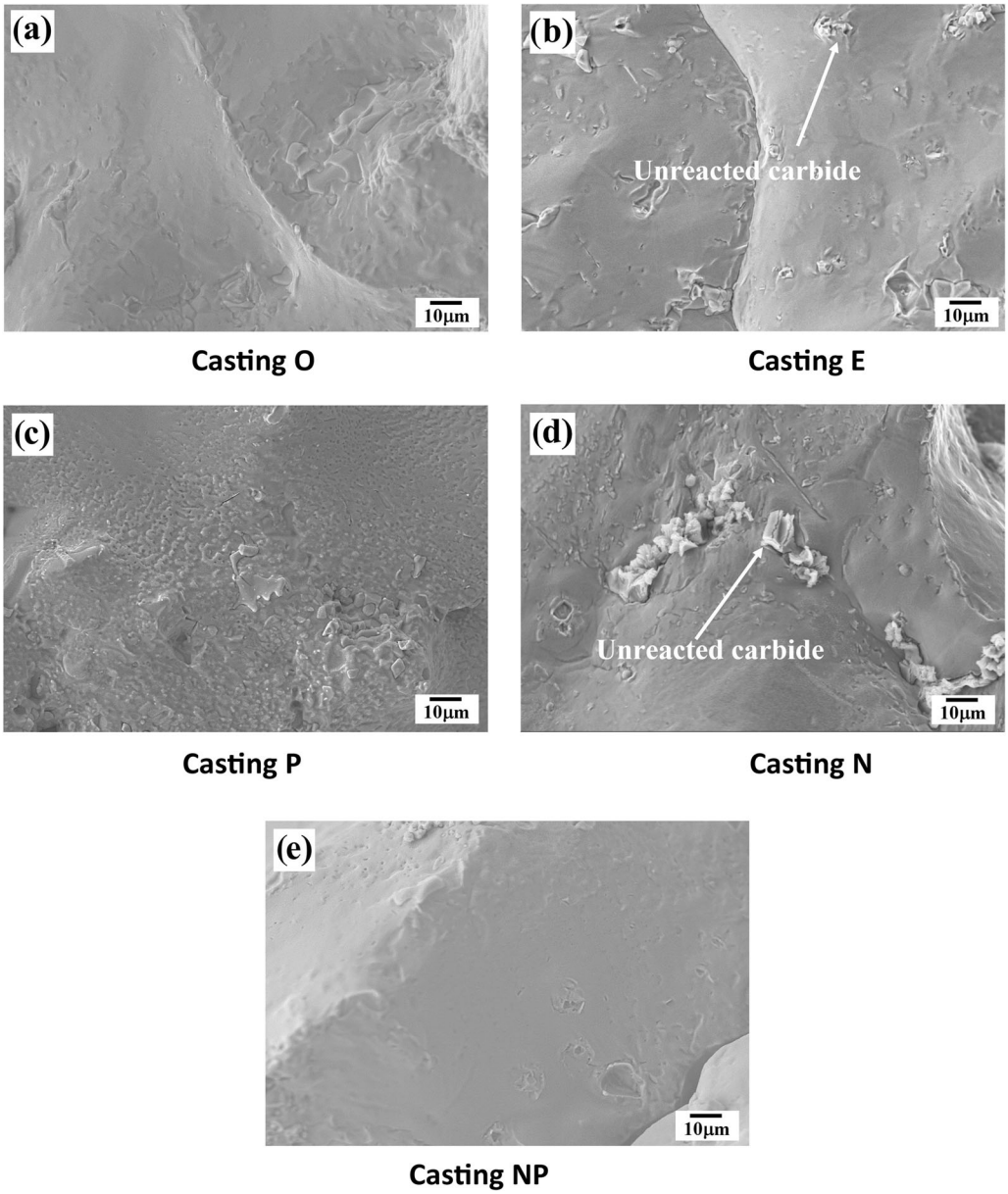

Fig. 8—Fracture surfaces of on-heating samples pulled at 1150 °C: (*a*) casting O, (*b*) casting E, (*c*) casting P, (*d*) casting N, and (*e*) casting NP.

Furthermore, in all on-cooling test samples pulled at 1150 °C, eutectic Laves phases were observed on the longitudinal cross sections close to NbC carbides (Figure 11). Such phases have also been observed by other researchers[10,25] and are believed to be artifacts of the on-cooling test that form after constitutional liquation of the NbC precipitates. Evidence of constitutional NbC liquation was observed on the fracture surface of casting P pulled at 1050 °C, revealing Nb-enriched areas close to NbC carbides (Figure 9(d)). The high Nb content of these areas provided favorable conditions for the precipitation of Laves phases upon subsequent cooling. The EDX-based analysis of the chemical composition of the eutectic Laves phases confirmed that they formed during the on-cooling process, because their chemical composition was close to that of the globular Laves phase detected in the as-cast samples (Table IX). After HIP and solution heat treatment, the globular interdendritic Laves phase observed in three of the castings had higher Mo (13.08 wt pct) than that in the as-cast state (Mo = 7.86 wt pct). This Mo enrichment during heat treatment has been attributed to the lower diffusivity of Mo in the austenite matrix compared to other elements composing the Laves phase.[18] Eutectic Laves phases associated with NbC constitutional liquation were observed in all samples tested at 1150 °C and may contribute to the null ductility determined at this temperature in on-cooling hot ductility tests for the different casting batches.

Therefore, apart from the melting of Laves phases, hot ductility is also affected by constitutional liquation of NbC carbides. Singh *et al.*[12] have suggested that constitutional liquation of MC carbides is affected by the solidus temperature and local concentration of Nb

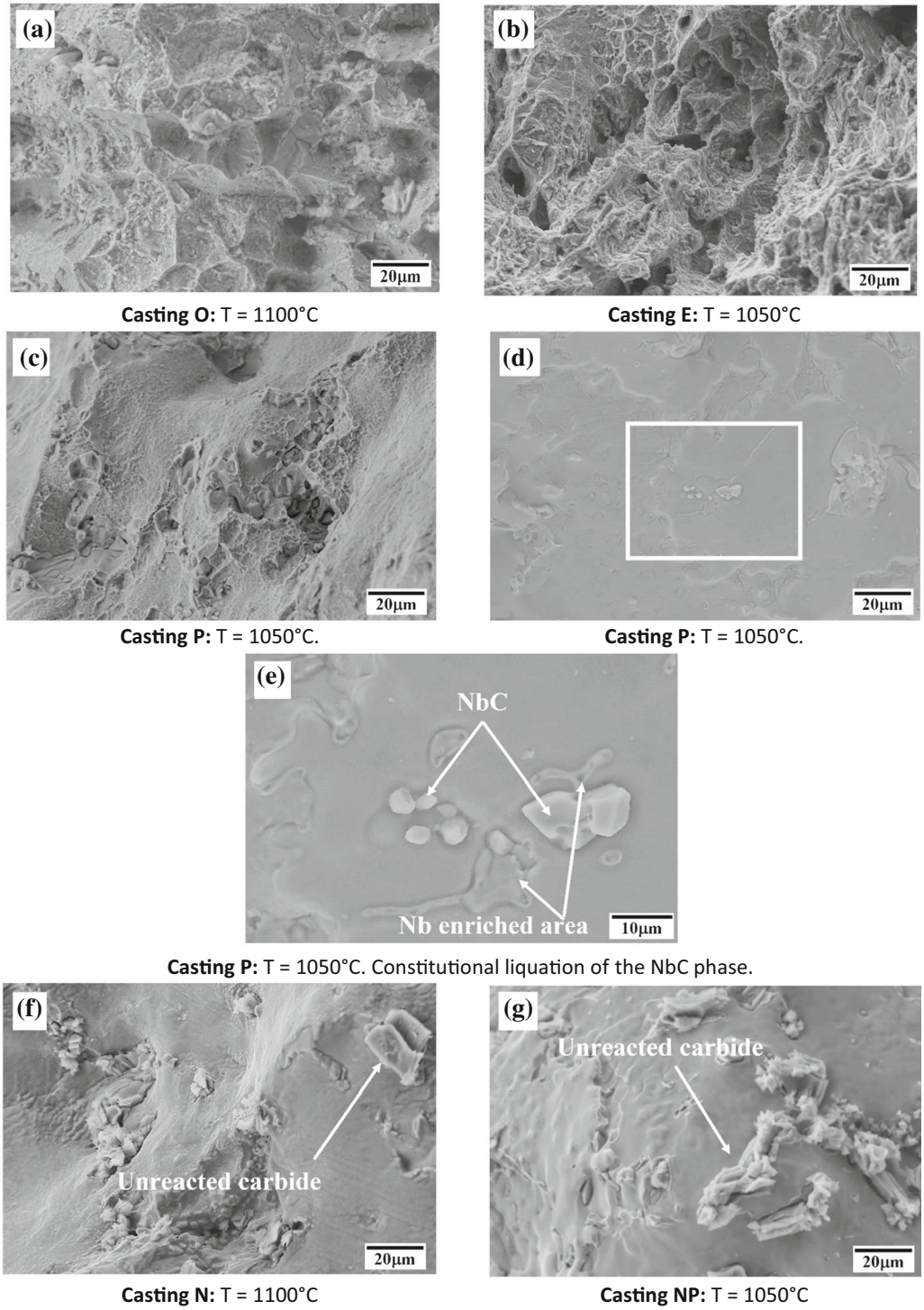

Fig. 9—Fracture surface of on-cooling samples (*a*) casting O, (*b*) casting E, (*c*) casting P: area with ductile features (*d*) casting P, showing area with liquid film present at the moment of fracture, (*e*) casting P: detail of (d), showing constitutional liquation of NbC with adjacent Nb-enriched areas, (*f*) casting N, and (*g*) casting N and (g) casting NP, showing evidence of liquation.

around the Nb carbides. They have attributed the extensive grain boundary melting observed in Nb homogenized samples to a lower solidus temperature because of the homogenization treatment.

To analyze the effects of Si and cooling rate on the solidus temperature and solidification range, we performed thermodynamic diffusion-based simulations and DSC measurements. Table X shows the solidus and liquidus temperatures obtained in simulations and experimental tests. With increasing Si content, the solidus temperature decreased, and the solidification range considerably increased. This tendency was also observed in the DSC experiments. The lowest solidification temperature determined by DSC was observed in

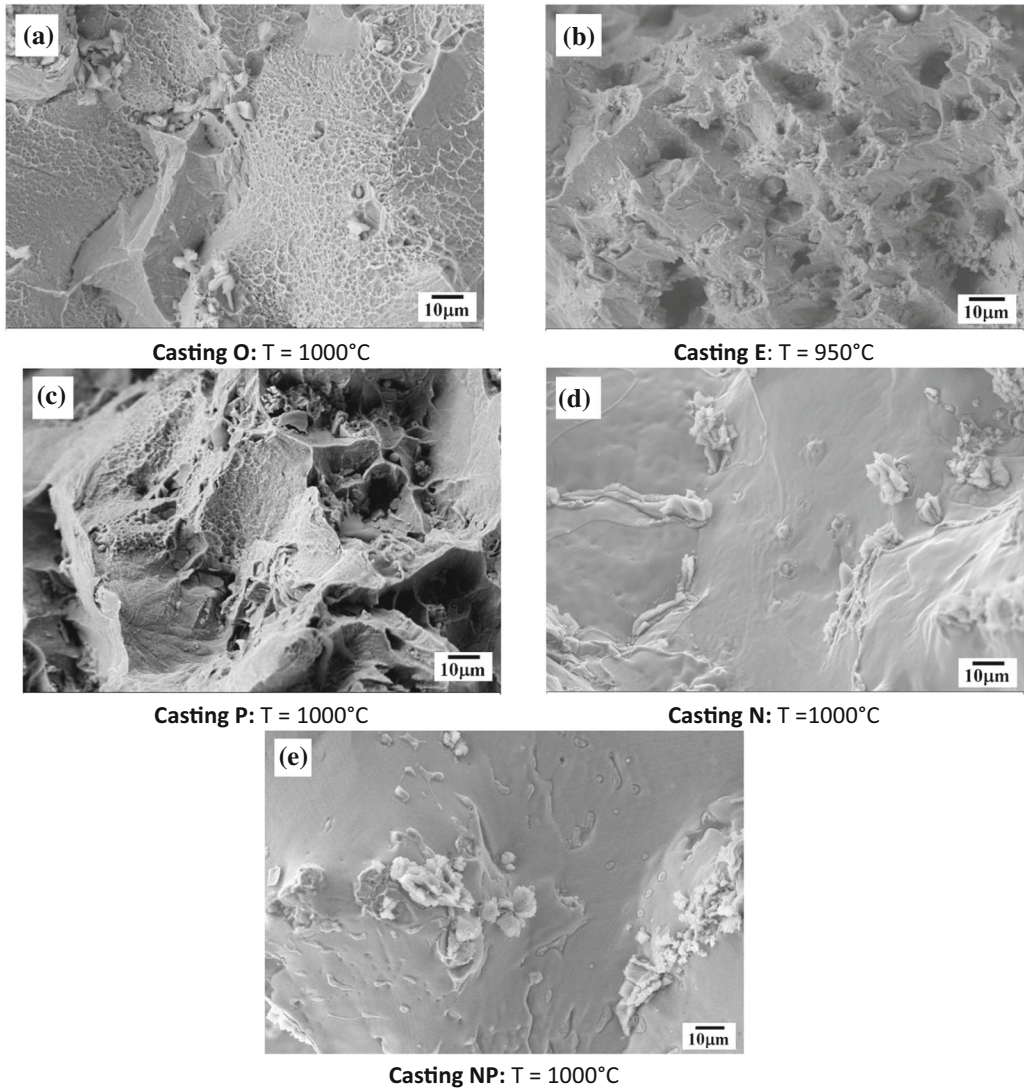

Fig. 10—Fracture surface of on-cooling samples. (*a*) casting O, (*b*) casting E, (*c*) casting P, (*d*) casting N, and (*e*) casting NP.

the high Si alloy, followed by the slowly solidified castings N and NP. Thus, in these castings (P, N, and NP), the hot ductility loss was affected by both Laves phase melting and the earlier onset of constitutional NbC liquation, due to their lower solidus temperatures, which in turn led to enhanced formation of liquid on the grain boundaries in the on-heating tests.

B. *Stress Rupture Tests*

Stress rupture samples of both castings (O and P) showed an intergranular fracture mode after exposure to a temperature of 650 °C and a stress of 689 MPa. In both castings, many fine disk-shaped γ'' precipitates, distributed uniformly over the γ matrix, were observed, thereby indicating that the aging heat treatment had been performed correctly. The difference in stress rupture life and ductility between castings O and P was explained by the different precipitates observed along the grain boundaries. Casting O (low Si content), with longer stress rupture life and higher elongation, showed serrated intergranular δ phase needles, whereas in casting P (high Si content), the grain boundary was decorated by a small rounded and elongated Laves phase (Figures 12 and 13). The latter casting also showed a secondary crack propagating along the grain boundary decorated with Laves phases (Figure 13). The chemical compositions of the different precipitates were determined through EDX spot analysis (Table XI). It is worth to mention that due to the small size of the precipitates, the analysis results might have been affected by interference of the EDX interaction volume with the matrix, and thus, certain amounts of matrix elements can appear in the chemical compositions of the precipitates. NbC carbides, δ and Laves phases had a higher Nb content than the γ matrix, and the Laves phases additionally a higher Mo and Si content. The NbC carbides had the highest Nb content and small quantities of other carbide-forming elements such as Ti, Cr, Fe, and Mo.

A plate-like δ-phase protruding from grain boundaries into the surrounding γ matrix grains has been

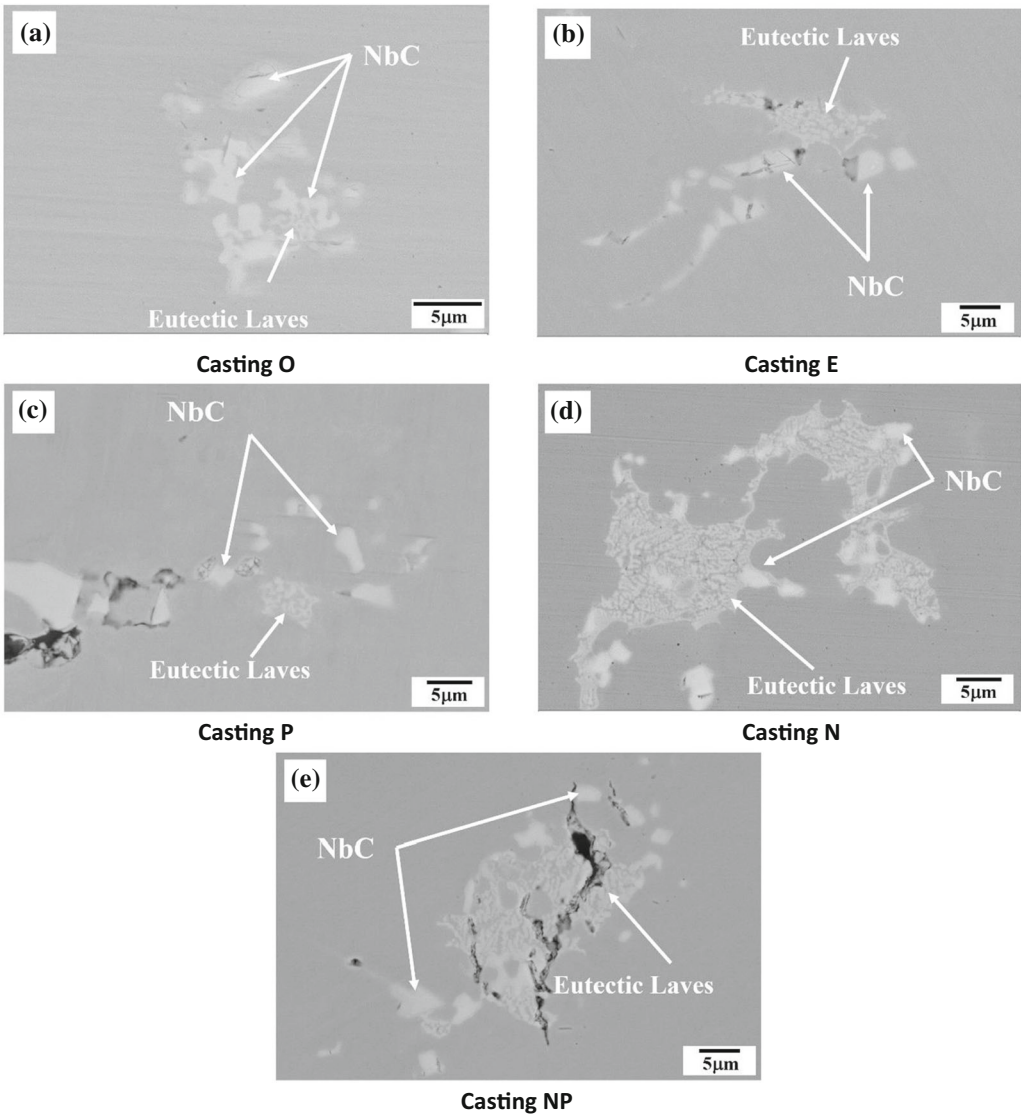

Fig. 11—Eutectic Laves phase observed at NbC carbides of on-cooling samples pulled at 1150 °C: (*a*) casting O, (*b*) casting E, (*c*) casting P, (*d*) casting N, and (*e*) casting NP. Longitudinal section.

Table IX. Chemical Compositions of Different Laves Phases Observed in Casting P Tested at $T = 1050$ °C in the Heat-Treated State (Homogenization (H) + Hot Isostatic Pressing (HIP) + Post-HIP + Solution Heat Treatment (S)) and in the As-Cast State

		Laves Phase Composition (Weight Percent)							
Morphology	State	Al	Si	Ti	Cr	Fe	Ni	Nb	Mo
Interdentric Globular	H + HIP + post-HIP + S	0.05	2.06	0.53	11.80	13.01	30.95	28.52	13.08
Eutectic Laves	H + HIP post-HIP + S	0.28	1.31	0.94	12.92	13.62	40.19	22.89	7.86
Interdentric Globular	as cast	0.13	1.29	0.95	11.15	11.95	34.63	32.11	7.80

reported to effectively divert initiation cracks from weak grain boundaries.[26,27] Moreover, the presence of brittle Laves phases with the same orientation as the grain boundary, could facilitate crack initiation and propagation. In a modified M718 alloy with high Mo content, Da-Wei *et al.*[28] have observed that crack initiation and propagation occur at the interface between the grain boundary Laves phase and the austenitic matrix, thus diminishing stress rupture properties. Crack propagation through Laves phases and diminished stress rupture

Table X. Solidus and Liquidus Temperatures Determined by Scheil Simulation and DSC Measurements

Ref.	Si (Weight Percent)	Cooling Rate	Laves Area Percent	Scheil Simulation			DSC					
							Heating			Cooling		
				T_{sol} (°C)	T_{liq} (°C)	ΔT (°C)	T_{sol} (°C)	T_{liq} (°C)	ΔT (°C)	T_{sol} (°C)	T_{liq} (°C)	ΔT (°C)
O	0.051	1.65	—	1120	1340	220	1239	1373	134	1223	1361	138
E	0.110	1.65	—	1100	1336	236	1235	1368	133	1211	1358	147
P	0.170	1.65	0.35	1078	1338	260	1227	1367	140	1207	1358	151
N	0.120	0.52	0.19	1100	1340	240	1231	1367	136	1215	1359	144
NP	0.120	0.52	0.14				1231	1368	137	1214	1356	142

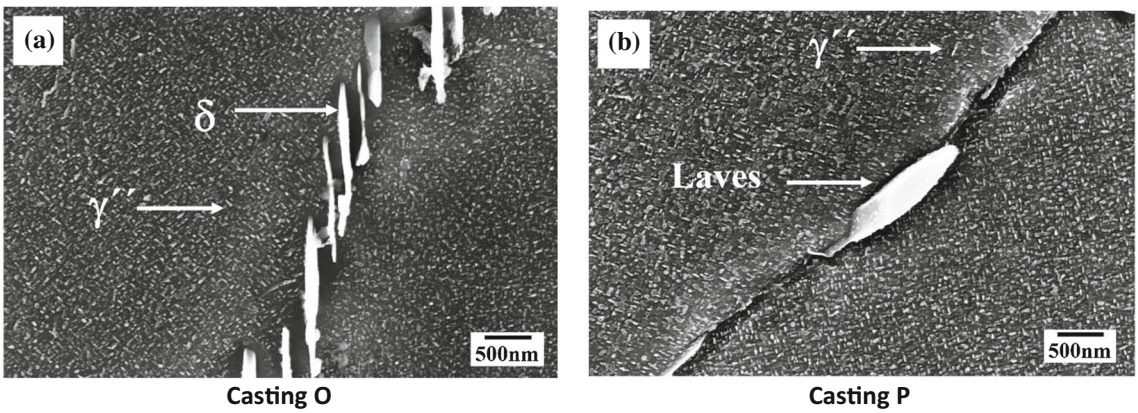

Fig. 12—Longitudinal cross sections showing the phases present at the grain boundaries in (*a*) casting O and (*b*) casting P.

properties in cast + HIP alloy 718 have also been reported by Schirra *et al.*[14]. However, in that study, Laves phases were located in the interdendritic region and had considerably larger sizes and volume fractions than those in the current study. No pronounced effects of grain boundary Laves phases on stress rupture properties have been observed in wrought materials.[13,14] Schirra *et al.*[14] believe that, in these materials, the high-temperature properties are more associated with the grain size than the presence of Laves phases on grain boundaries. But in investment castings, the grain size is much larger and could provide a less torturous crack propagation path; thus, the presence of grain boundary Laves phases is expected to be more evident.

The formation of grain boundary Laves phases is associated with the Si content. Si is well known to promote the formation of Laves phases. Increasing the Si content leads to a greater volume fraction and apparently increases the stability of the primary Laves phase.[6,14,18] With increasing Si content in the alloy, the Si content in the Laves phase also increases and is higher than that of the matrix. Furthermore, higher Si content (0.21 wt pct or higher) has been reported to promote the formation of Laves and MC phases on grain boundaries and to decrease the precipitation of intergranular δ phase.[13,29] In the current study, grain boundary Laves phases were observed only in casting P, which had the highest Si content of 0.17 wt pct, whereas the other alloys revealed δ phases on the grain boundary. Guo *et al.*[13] have suggested the following explanation for the suppression of δ phase precipitation: after homogenizing treatment, the Si content in the matrix increases because of the dissolution of the primary Laves phase, thus resulting in more severe lattice strain and a large driving force for diffusion of Si into the grain boundary during thermomechanical processing and heat treatment. With increasing Si content, the segregation of Si at the grain boundary is enhanced. The Laves and MC phases with a high Si content nucleate more easily at the grain boundary than the δ phase with low Si content.

V. CONCLUSIONS

In the present work, the influence of different Si contents (0.051, 0.11, and 0.17 wt pct), solidification rates (0.52 °C/s and 1.65 °C/s), and pre-weld heat treatment (2 h of additional solution heat treatment before HIP) on the microstructure and high-temperature properties (hot ductility and stress rupture) were investigated in alloy 718 investment castings. The following conclusions can be drawn:

- The Laves phase content in the as-cast states increased with increasing Si content and decreasing solidification rate.

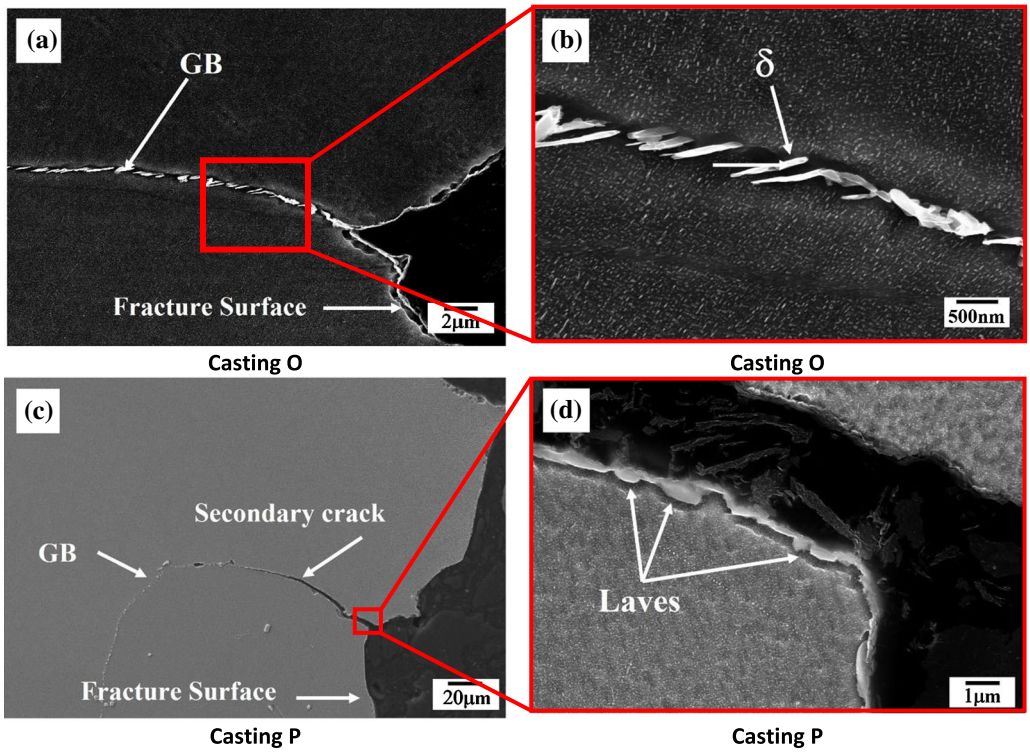

Fig. 13—Longitudinal cross section of stress rupture samples, showing the morphology of the phases precipitated on the grain boundaries (GB) close to the fracture surface (*a*) and (*b*) casting O and (*c*) and (*d*) casting P, presenting a secondary crack propagating along the grain boundary.

Table XI. Chemical Compositions (in Wt Percent) of Different Phases Observed in the Longitudinal Cross Sections, Obtained Through EDX Analysis

Phase	Location	Phase Composition (Weight Percent)							
		Al	Si	Ti	Cr	Fe	Ni	Nb	Mo
γ	matrix	0.12	0.14	0.87	18.13	21.01	50.99	5.10	3.25
NbC	grain boundary	0.01	0.08	7.24	0.97	1.01	2.13	87.24	1.30
δ (Figure 12(a))	grain boundary	0.36	0.32	1.35	14.51	16.62	52.82	11.41	2.61
Laves (Figure 12(b))	grain boundary	0.28	1.80	0.79	14.53	17.58	37.26	18.24	9.53
Laves (Figure 13(d))	grain boundary laves present at secondary crack	0.35	1.60	0.72	15.40	18.28	41.08	14.75	7.83

- After homogenization, HIP, and solution heat treatment, residual content of Laves phase (≤ 0.35 pct in area) was observed only in the samples with highest Si content (0.17 wt pct) and slow solidification rate (0.52 °C/second). In the slowly solidified castings, the application of an additional pre-HIP heat treatment for 2 hours at 1052 °C was not sufficient to eliminate the Laves phase completely.
- Small amounts of residual Laves phases (0.14 to 0.35 wt pct) adversely affect both hot ductility and stress rupture properties.
- Hot ductility tests indicated that the presence of residual Laves phase led to an earlier decrease in hot ductility in on-heating tests and retarded ductility recovery in on-cooling tests.
- In castings with high Si content (0.17 wt pct) and low solidification rate (0.52 °C/second), incipient melting of Laves phases contributed to the early ductility decrease. The ductility loss in samples with low and conventional Si content (0.051 and 0.11 wt pct) was attributed to constitutional NbC liquation.
- In on-cooling tests of samples with the highest Si content (0.17 wt pct), the lower ductility recovery temperature (DRT) and expanded brittle temperature range (BTR) were attributed to areas with persistent grain boundary liquation observed on the fracture surface due to the incipient melting of the residual Laves phase.
- In the slowly solidified samples, with coarser grain sizes and smaller aspect ratios, the very slow recovery rate and very limited ductility recovery capability were associated with longer liquid continuity along grain boundaries after incipient melting and constitutional NbC liquation.

Stress rupture properties

- Stress rupture properties (life and ductility) decreased by approximately 30 pct when the Si content was raised from 0.051 to 0.17 wt pct. This decrease was attributed to the formation of a semicontinuous network of elongated Laves phase along grain boundaries. The sample with low Si content had serrated intergranular δ phase needles protruding from grain boundaries into surrounding matrix grains. This microstructure was more effective in preventing crack initiation and propagation along grain boundaries than the one with Laves phase on the grain boundaries.

ACKNOWLEDGMENTS

This research was performed partially under the framework of the HiperTURB project, which was funded by the Clean Sky 2 Joint Undertaking under the European Union's Horizon 2020 research and innovation program, Grant Agreement No. 755561. Bengt Pettersson and Vikström Fredrik from the GKN Aerospace company in Trollhättan (Sweden) are gratefully acknowledged for their technical support and fruitful discussions. Additionally, the authors thank Kejll Hurtig and Joel Andersson (Department of Engineering Science at West University) for support in performing hot ductility tests. This study was completed with financial support from the Basque Government (Project: CEMAP: Desarrollo de Materiales Cerámicos y Metálicos de Altas Prestaciones para Fabricación Avanzada, ELKARTEK KK-2020/00047 and MINERVA: ELKARTEK KK-2022/00082).

AUTHOR CONTRIBUTIONS

AN contributed to investigation of stress rupture tests, methodology, formal analysis, and writing—original draft preparation. RGM contributed to investigation of stress rupture tests, and microstructural investigation and visualization. FS contributed to conceptualization, methodology, supervision, writing—review and editing, project administration, and funding acquisition. PPR contributed conceptualization, methodology, investigation in investment casting, and writing—review. AC contributed to investigation of hot ductility tests, microstructural investigation, and visualization. DB contributed to DSC measurements. LV contributed to investigation of hot ductility tests, methodology, data curation, and visualization. PA contributed to investigation of hot ductility, methodology, formal analysis, and writing—original draft preparation. All authors have read and agreed to the published version of the manuscript.

CONFLICT OF INTEREST

The authors declare that they have no known competing financial interests or personal relationships that could have appeared to influence the work reported herein.

REFERENCES

1. M.J. Donachie and S.J. Donachie: *Superalloys: A Technical Guide*, 2nd ed. ASM International, Novelty, OH, 2002, pp. 1–38.
2. J.F. Radavich: *Superalloy 718-Metallurgy and Applications*, The Minerals, Metals & Materials Society, Warrendale, PA, 1989, pp. 229–40.
3. X. Liang, R. Zhang, Y. Yang, and Y. Han: *Superalloys 718, 625, 706 and Various Derivatives*, The Minerals Metals & Materials Society, Warrendale, PA, 1994, pp. 947–56.
4. Z.J. Miao, A.D. Shan, Y.B. Wu, J. Lu, W.L. Xu, and H.W. Song: *Trans. Nonferrous Met. Soc. China*, 2011, vol. 21, pp. 1009–017.
5. W.D. Cao, R.L. Kennedy, and M.P. Willis: *Superalloys 718, 625, and Various Derivative*, Metals and Materials Society, Warrendale, PA, The Minerals, 1991, pp. 147–60.
6. B.G. Muralidharan, V. Shankar, and T.P.S. Gill: *Weldability of Inconel 718-A Review*, Indira Gandhi Centre for Atomic Research, Kalpakkam, Tamil Nadu, 1996.
7. R.G. Thompson and S. Genculu: *Weld. J.*, 1983, vol. 62, pp. 337–45.
8. S. Singh and J. Andersson: *Sci. Technol. Weld. Join.*, 2018, vol. 23, pp. 568–74.
9. S. Singh, F. Hanning, and J. Andersson: *Metall. Mater. Trans. A*, 2020, vol. 51A, pp. 6248–257.
10. J. Andersson, G.P. Sjöberg, L. Viskari, and M.C. Chaturvedi: *Mater. Sci. Technol.*, 2012, vol. 28, pp. 609–19.
11. J. Andersson, G.P. Sjöberg, L. Viskari, and M. Chaturvedi: *Mater. Sci. Technol.*, 2012, vol. 28, pp. 733–41.
12. S. Singh, F. Hanning, and J. Andersson: *Mater. Sci. Eng. A*, 2021, vol. 799, p. 140151.
13. S. Guo, W. Sun, D. Lu, and Z. Hu: *Superalloys 718, 625, 706 and Various Derivatives*, The Minerals, Metals & Materials Society, Warrendale, PA, 1997, pp. 521–30.
14. J.J. Schirra, R.H. Caless, and R.W. Hatala: *Superalloys 718, 625 and Various Derivatives*, The Minerals, Metals & Materials Society, Warrendale, PA, 1991, pp. 375–88.
15. E. Hosseini and V.A. Popovich: *Addit. Manuf.*, 2019, vol. 30, p. 100877.
16. V.A. Popovich, E.V. Borisov, V. Heurtebise, T. Riemslag, A.A. Popovich, and V.S. Sufiiarov: *TMS 147th Annual Meeting & Exhibition Supplemental Proceedings*, Springer, Cham, 2018, pp. 85–97.
17. S. Sui, H. Tan, J. Chen, C. Zhong, Z. Li, W. Fan, A. Gasser, and W. Huang: *Acta Mater.*, 2019, vol. 164, pp. 413–27.
18. P. Álvarez, A. Cobos, L. Vázquez, N. Ruiz, P.P. Rodríguez, A. Magaña, A. Niklas, and F. Santos: *Metals*, 2021, vol. 11, p. 402.
19. J.J. Schirra: *Superalloys 718, 625, 706 and Various Derivatives*, The Minerals, Metals & Materials Society, Warrendale, PA, 1997, pp. 439–66.
20. ISO/TR 17641-3:2005(E) Destructive Tests on Welds in Metallic Materials-Hot Cracking Tests for Weldments-Arc Welding Processes-Part 3: Externally Loaded Tests, International Organization for Standardization (ISO), Geneva, 2005.
21. R.G. Thompson, J.R. Dobbs, and D.E. Mayo: *Weld. J.*, 1986, vol. 65, pp. 299–304.
22. J.N. DuPont, J.C. Lippold, and S.D. Kiser: *Welding Metallurgy and Weldability of Nickel-Base Alloys*, Wiley, Hoboken, NJ, 2009.
23. W.A. Baeslack III. and D.E. Nelson: *Metallography*, 1986, vol. 19, pp. 371–79.
24. I. Woo, K. Nishimoto, K. Tanaka, and M. Shirai: *Weld. Int.*, 2000, vol. 14, pp. 514–22.
25. S. Benhadad, N.L. Richards, and M.C. Chaturvedi: *Metall. Mater. Trans. A*, 2002, vol. 33A, pp. 2005–017.
26. L. Shuqi, Z. Jingyun, Y. Jinyan, Q. Deng, and J. Du: *Superalloys 718, 625, 706 and Various Derivatives*, The Minerals, Metals & Materials Society, Warrendale, PA, 1994, pp. 545–5.

27. G. Sjoberg and N.G. Ingesten: *Superalloys 718, 625 and Various Derivatives*, The Minerals, Metals & Materials Society, Warrendale, PA, 1991, pp. 603–20.
28. D.-W. Han, L.-X. Yu, F. Liu, B. Zhang, and W.-R. Sun: *Metall. Sin. (Engl. Lett.)*, 2018, vol. 31, pp. 1224–32.
29. M.G. Burke and M.K. Miller: *Superalloys 718, 625 and Various Derivatives*, The Minerals, Metals & Materials Society, Warrendale, PA, 1991, pp. 337–50.